

Comparison of critical adsorption scaling functions obtained from neutron reflectometry and ellipsometry

M. D. Brown and B. M. Law

Condensed Matter Laboratory, Department of Physics, Kansas State University, Manhattan, Kansas 66506-2601

S. Satija

National Institute of Standards and Technology, Gaithersburg, Maryland 20899

W. A. Hamilton

Condensed Matter Sciences Division, Oak Ridge National Laboratory, Oak Ridge, Tennessee 37831-6393

E. Watkins

Los Alamos National Laboratory, Los Alamos, New Mexico 87545

J.-H. J. Cho

Condensed Matter Sciences Division, Oak Ridge National Laboratory, Oak Ridge, Tennessee 37831-6393

J. Majewski

Los Alamos National Laboratory, Los Alamos, New Mexico 87545

(Received 22 November 2006; accepted 10 April 2007; published online 24 May 2007)

Carpenter *et al.* [Phys. Rev. E **59**, 5655 (1999); **61**, 532 (2000)] managed to explain ellipsometric critical adsorption data collected from the liquid-vapor interface of four different critical binary liquid mixtures near their demixing critical temperature using a single model. This was the first time a single universal function had been found which could quantitatively describe the surface critical behavior of many different mixtures. There have also been various attempts to investigate this surface critical behavior using neutron and x-ray reflectometries. Results have been mixed and have often been at variance with Carpenter *et al.* In this paper, the authors show that neutron reflectometry data collected from a crystalline quartz-critical mixture interface, specifically deuterated water plus 3-methylpyridine, can be quantitatively explained using the model of Carpenter *et al.* derived from ellipsometric data. © 2007 American Institute of Physics.

[DOI: 10.1063/1.2736383]

I. INTRODUCTION

At a solid-liquid or liquid-vapor interface of a binary fluid mixture there will in general be an adsorbed film in which the relative volume fraction of the components will differ significantly from the bulk composition. This adsorption is driven by a surface field h_1 , which results from the difference in surface tensions of the components at that interface, where the component possessing the lower surface tension is more abundant in the adsorbed film compared with the bulk. Over length scales of $\sim 10\xi$, where ξ is the composition correlation length, the adsorbed film will decay to the bulk composition. Various phenomena, such as catalysis, electrolysis, and the permeability of membranes, can be influenced by the presence and structure of an adsorbed film.¹

For the special case of a critical binary fluid mixture, which undergoes a bulk second order phase transition from an ordered phase separated state (the two phase region) to a disordered mixed state (the one phase region) at a critical temperature T_c , Fisher and de Gennes² postulated that the adsorption profile $\phi(z)$ at the interface would exhibit interesting universal, system independent behavior sufficiently close to T_c . $\phi(z)$ is expected to depend upon two variables, a dimensionless depth z/ξ and the surface field h_1 . If h_1 is sufficiently large so that the component possessing the low-

est surface tension completely saturates the surface [i.e., $\phi(0)=1$], then the adsorption profile becomes independent of h_1 . In this strong critical adsorption regime the dependence of $\phi(z)$ upon z/ξ is usually defined using a local order parameter,

$$m_{\pm}(z) = \phi(z) - \phi_c, \quad (1)$$

where the universal surface scaling behavior can be described by

$$m_{\pm}(z) = M_{\pm} t^{\beta} P_{\pm}[(z + z_c)/\xi_{\pm}]. \quad (2)$$

In these equations ϕ refers to the volume fraction of the preferentially adsorbed component as a function of distance z from the interface and ϕ_c is the bulk critical volume fraction. The coexistence curve, described by $M_{\pm} t^{\beta}$, separates the one phase region from the two phase region of the binary fluid mixture while the correlation length $\xi = \xi_0 t^{-\nu}$ with reduced temperature $t = |T - T_c|/T_c$, where the bulk critical exponents $\beta \approx 0.328$ and $\nu \approx 0.632$.³ M_{\pm} and ξ_0 are system dependent parameters. The universal surface scaling function P exhibits differing values in the one phase region (subscript +) compared with the two phase region (subscript -).

For strong critical adsorption m must remain finite and nonzero at the critical temperature ($t=0$); hence, m must lose its t dependence for sufficiently small $x=z/\xi \ll 1$. This can only occur if²

$$P_{\pm}(x) \sim c_{\pm} x^{-\mu}, \quad \mu = \beta/\nu. \quad (3)$$

The extrapolation length z_e , which appears in Eq. (2), prevents $P(x)$ from diverging at $z=0$. This power law behavior eventually crosses over to an exponential decay

$$P_{\pm}(x) \sim P_{\pm}(\infty) + P_{\infty\pm} e^{-x} \quad (4)$$

at sufficiently large x where, because $P(x)$ is a universal function, c_{\pm} and $P_{\infty\pm}$ will be universal numbers. In order that Eq. (4) correctly describes the bulk order parameter at $z \rightarrow \infty$, we must additionally have

$$P_{+}(z \rightarrow \infty) \equiv P_{+}(\infty) = 0, \quad (5)$$

$$P_{-}(z \rightarrow \infty) \equiv P_{-}(\infty) = 1. \quad (6)$$

It has taken many, many years to determine a universal form for $P(x)$ which could describe the experimental results of many different critical liquid mixtures. In 1999 Carpenter *et al.*⁴ finally found a form for $P(x)$ which could describe the ellipsometric critical adsorption results measured at the liquid-vapor interface of a number of different critical liquid mixtures. However, a disturbing feature which continues to plague this field is that $P(x)$ determined using other experimental techniques, such as neutron and x-ray reflectometries, often disagree with each other and also disagree with the form determined via ellipsometry. The primary purpose of this paper is to compare a careful neutron reflectometry experiment measured at the crystalline quartz-critical binary liquid mixture surface with $P(x)$ determined via ellipsometry.

It is important to prove that $P(x)$ is indeed universal and that the same functional form can describe the experimental results from many different critical binary liquid mixtures measured via many different experimental techniques because $P(x)$ serves as the basis for determining many other universal functions. For example, if the surface field h_1 is small, then the surface composition $\phi(z)$ will depend not only upon the dimensionless depth $x=z/\xi$ but also upon h_1 , where, in this weak critical adsorption regime, the local order parameter $m_{\pm}(z)$ will be described by a different universal function $G(x, h_1)$ (Refs. 5 and 6) which will reduce to $P(x)$ in the limit of large h_1 . The determination of $G(x, h_1)$ is predicated upon a reliable determination of $P(x)$.⁷ In a similar manner, if one of the components is highly polar, then one finds that both the local surface composition and local orientational order vary with $x=z/\xi$, where the latter is caused by the interaction between the dipole and its image when in the vicinity of a surface.⁸ Determination of this surface orientational order is also dependent upon an accurate knowledge of $P(x)$.⁹

This publication is set out as follows. In Sec. II we survey prior work on strong critical adsorption and summarize the ellipsometric measurements for the $P(x)$ function. The experimental methods and analysis are described in Secs. III and IV, respectively. A summary is presented in Sec. V.

II. SURVEY OF PRIOR WORK

There are a number of key developments in our understanding of critical adsorption. A brief historical perspective of these developments is given below. This survey of prior work will enable the reader to better understand the motivation for the current paper.

The first experimental observation of the effects of strong critical adsorption was made by Rusanov¹⁰ using the technique of ellipsometry. This work has largely gone unnoticed by later workers with the exception of Beaglehole.¹¹ Surprisingly this first observation predates the theoretical predictions of Fisher and de Gennes.² In this early work Rusanov observed a divergence in the relative surface adsorption, defined as

$$\Gamma = \int [m(z) - m(\infty)] dz. \quad (7)$$

The divergence in Γ is caused by the fact that $m(z)$ scales with z/ξ , where, according to Eq. (2),

$$\Gamma \sim P_{\pm} t^{\beta-\nu}, \quad (8)$$

with a universal integral

$$P_{\pm} = \int [P_{\pm}(x) - P_{\pm}(\infty)] dx,$$

which takes differing values in the one and two phase regions.

The theoretical predictions of Fisher and de Gennes, encapsulated in Eqs. (2) and (3), stimulated a significant experimental effort using a variety of experimental techniques, including ellipsometry,¹²⁻¹⁵ evanescent-wave reflectometry,^{16,17} light scattering,¹⁸ and volumetry¹⁹ to elucidate the functional form of $P(x)$. Ellipsometry provides a direct measure of Γ (at least far from T_c),²⁰ while the other techniques provide other (integral) measures over $P(x)$.¹⁶⁻¹⁸ The variation of $P(x)$ with x (which is hidden inside these universal integrals) can only be ascertained indirectly by getting sufficiently close to T_c ($t \lesssim 10^{-3}$) where ξ is sufficiently large so that, for the optical measurements, interference effects provide a nonlinear measure of $P(x)$ via a solution of Maxwell's equations.

The universality of $P(x)$ was not fully appreciated until the work of Liu and Fisher²¹ who compared experimental measurements on *two different* critical mixtures to see if a single functional form for $P(x)$ could describe both experiments. As appropriate models incorporating both Eqs. (3) and (4), they considered the exponential Pade (EP) model,

$$P(x) = c_{+} \left(\frac{1}{1 - e^{-x}} + \left(\frac{c_{+}}{P_{\infty+}} \right)^{-\nu/\beta} \right)^{\beta/\nu} e^{-x}, \quad (9)$$

and the power law-exponential model,

$$P(x) = c_{+} \left(\frac{1}{x} + \left(\frac{c_{+}}{P_{\infty+}} \right)^{-\nu/\beta} \right)^{\beta/\nu} e^{-x}. \quad (10)$$

These functional forms have the advantage that they are continuous for all x . However, they are strictly only applicable in the one phase region because neither of these equations re-

TABLE I. Critical adsorption parameters. (The following abbreviations have been used in this table: MC^{*}=methanol+deuterated cyclohexane, BW^{*}=2-butoxyethanol+deuterated water, FH=*n*-hexane + perfluorohexane, CM^{*}=cyclohexane + deuterated methanol, H^{*}F=*d*-hexane + perfluorohexane, W^{*}P=deuterated water+3-methylpyridine, and DT=*n*-dodecane + tetrabromoethane.)

Technique	Liquid mixture/substrate	c_+	$\mu=\beta/\nu$
RG ^a	Theory	0.717	
MC ^b	Theory	0.866	
Interpolation ^c	Theory	0.94±0.05	
Local functional ^d	Theory	0.857	
Optical ^c	Various/air or glass	0.955±0.08	
Ellipsometry-P1 ^c	Various/air	0.788 ^{+0.009} _{-0.015}	
Ellipsometry-EP ^c	Various/air	0.817	
Neutron ^f	MC [*] /air	0.34	0.52
Neutron ^g	BW [*] /Si	0.11	0.53±0.02
Neutron ^h	FH/air	1.78±0.2	0.54±0.03
Neutron ^h	CM [*] /air	0.94±0.15	0.46±0.03
Neutron ^h	MC [*] /air	0.97±0.15	0.49±0.05
Neutron ⁱ	H [*] F/Si	0.90±0.04	0.514±0.018
Neutron ^j	W [*] P/quartz	0.788 ^k	0.519 ^k
X ray ^l	DT/air	1.87	

^aReference 22.

^bReference 23.

^cReference 25.

^dReference 24.

^eReference 4.

^fReference 30.

^gReference 31.

^hReference 32.

ⁱReference 33.

^jThis work.

^kFrom use of the P1 model.

^lReference 34.

duce to Eq. (6), applicable in the two phase region, in the limit of large x . Liu and Fisher found that the universal crossover length scale $c_+/P_{\infty+} \approx 1.2$ in the one phase region by comparison with the evanescent-wave reflectometry results of Schlossman *et al.*¹⁷ and ellipsometry results of Schmidt and Moldover.¹⁴

Theoretical estimates for the actual functional form of $P(x)$ have been derived in three dimensions using renormalization group²² (RG) (to first order in $\epsilon=4-d$), Monte Carlo simulations (MC),²³ and local functional theory.²⁴ The local functional theory results were found to be in excellent agreement with both the RG and MC calculations. However, Smith and Law²⁶ found that neither the RG nor MC functional forms for $P(x)$ could quantitatively explain experimental ellipsometric data.

Another key measure, providing evidence for universality, is the value of the universal number c_+ , which appears in Eq. (3). Flöter and Dietrich²⁵ reanalyzed a large number of earlier optical experimental measurements of strong critical adsorption to obtain an experimental estimate for $c_+ = 0.955 \pm 0.08$ (Table I). This experimental estimate com-

pared favorably with various theoretical estimates (Table I) including RG,²² MC,²³ interpolation,²⁵ and local functional²⁴ estimates. One should note, however, that approximate agreement of the universal number c_+ from optical experiments with RG and MC estimates does not necessarily imply that the full functional forms from RG or MC for $P(x)$ can quantitatively describe experimental data, as noted above.²⁶ Part of the problem is that Eqs. (3) and (4) only represent the leading order terms. Higher order terms are expected to take the form

$$P_{\pm}(x) = c_{\pm}x^{-\beta/\nu} + c_{1\pm}x^{(1-\beta)/\nu} + c_{2\pm}x^{(2-\beta)/\nu} + c_{3\pm}x^{3-\beta/\nu} + \dots, \quad (11)$$

at small x .²² At large x , Liu and Fisher²¹ suggested that

$$P_{\pm}(x) = P_{\pm}(\infty) + P_{\infty\pm}e^{-x} + P_{1\pm}e^{-2x} + P_{2\pm}e^{-3x} + \dots. \quad (12)$$

A more refined local functional theory analysis by Borjan and Upton²⁴ indicates that, for symmetry reasons, the large x expansion should be

$$P_{+}(x) = P_{+}(\infty) + P_{\infty+}e^{-x} + P_{2+}e^{-3x} + \dots \quad (13)$$

in the *one phase region*, where only odd powers of e^{-x} are present. The presence of these higher order corrections at small and large x , therefore, necessarily influences the determination of c_{\pm} . Carpenter *et al.*⁴ used a modified version of Eqs. (11) and (12), called the “P1 model,” where

$$P_{\pm}(x) = c_{\pm}x^{-\beta/\nu} + c_{1\pm}x^{(1-\beta)/\nu}, \quad x < x_0, \quad (14)$$

$$P_{\pm}(x) = P_{\pm}(\infty) + P_{\infty\pm}e^{-x} + P_{1\pm}e^{-2x}, \quad x \geq x_0, \quad (15)$$

to reexamine whether or not the ellipsometric data of Smith²⁰ for four different critical mixtures could be fitted with a single universal function. [For historical reasons, in the one phase region, Eq. (15) is a truncation of Eq. (12) rather than the more accurate Eq. (13).] In Eqs. (14) and (15) there are nine parameters c_{\pm} , $c_{1\pm}$, $P_{\infty\pm}$, $P_{1\pm}$, and x_0 that need to be determined, where x_0 is a crossover parameter which separates the power law region from the exponential region. Carpenter *et al.* used the continuity of $P_{\pm}(x)$ and $dP_{\pm}(x)/dx$ at x_0 , continuity of $m(z)$ at T_c plus three experimental constraints to reduce the number of adjustable parameters from nine to just one, specifically x_0 . By adjusting this single universal parameter x_0 , Carpenter *et al.* described the critical adsorption behavior for four different critical liquid mixtures in both the one and two phase regions. The values for these nine parameters, determined from ellipsometric data, are given in Table II. This universal functional form for $P(x)$ found by Carpenter *et al.* also described the ellipsometric data for a nonpolar critical liquid mixture at the liquid-vapor surface²⁷ and a critical mixture in contact with a molecularly

TABLE II. Critical adsorption scaling function models (from Ref. 4).

Model	Phase	$x_{0\pm}$	c_{\pm}	$c_{1\pm}$	$P_{\infty\pm}$	$P_{1\pm}$	$10^4\sigma$
P1	1	1.15	0.788 ^{+0.009} _{-0.015}	-0.245	0.963 ^{+0.117} _{-0.201}	1.437	1.3756
	2	1.15	1.117 ^{+0.013} _{-0.021}	0.169	0.572 ^{+0.357} _{-0.152}	0.533	
EP	1		0.817		1.035		1.5492

smooth Si wafer surface.²⁸ Carpenter *et al.* also fitted the one phase ellipsometric data of Smith using the exponential Pade model [Eq. (9) and Table II] and found reasonable but a slightly poorer fit (as indicated by the value of the standard deviation σ) compared with the P1 model. It is important to note that the value of c_+ =0.788 (Table II) for the P1 model agrees reasonably well with the exponential Pade estimate (c_+ =0.817, Table II), earlier optical experiments (c_+ ~0.955±0.08,²⁵ Table I), and theoretical estimates (c_+ ~0.717–0.94,^{22,23,25} Table I). The difference between c_+ for the P1 model and the optical and theoretical estimates could be due to the presence of the higher order terms in Eqs. (14) and (15). One can safely state that the leading order amplitude c_+ from visible light optical experiments and theory lies in the range c_+ ~0.72–0.96.

Theoretical work by Dietrich and Schack²⁹ suggested that both the amplitude c_+ and exponent μ of the power law critical adsorption behavior [Eq. (3)] could be measured directly via neutron or x-ray reflectometry. This paper stimulated a number of experimental attempts at measuring these parameters, as summarized in Table I. However, the values determined for c_+ ~0.1–1.9 from neutron^{30–33} and x-ray³⁴ experiments fall in a much broader range than found from visible light optical experiments. The recent neutron reflectometry experiment of Bowers *et al.*³³ seems to be in closest conformity to theoretical expectations. However, as mentioned above, agreement of c_+ from experiments with RG and MC estimates does not necessarily imply that the RG and MC models for $P(x)$ will be able to quantitatively explain experimental data. Here we compare the P1 model for $P(x)$, which quantitatively described ellipsometric data,⁴ with a neutron reflectometry experiment of strong critical adsorption.

For completeness, we should mention one further theoretical approach to critical adsorption before proceeding on to describe the neutron experiments. The scaling regime described by Ising critical exponents, and embodied in Eqs. (2) and (3), is only valid when fluctuations are important. Outside the scaling regime, the thermodynamic behavior is described by mean field concepts. Kiselev *et al.*³⁵ developed a (complicated) crossover adsorption theory which incorporates both the crossover in surface behavior as well as the crossover in bulk behavior. Ising behavior is found at $|t| \ll Gi$, close to T_c , and for distances $z \gg \xi_0 Gi^{-\nu}$. This behavior crosses over to the mean field behavior at $|t| \gg Gi$, far from T_c . Here Gi is the Ginzburg number. A study of a series of noncritical liquid mixtures of aniline plus cyclohexane³⁶ indicated that Gi lies in the broad range $0.0005 < Gi < 0.005$. This crossover adsorption theory is perhaps most useful for describing off critical liquid mixtures over a wide temperature and composition range. The concepts within this theory should also be applied to critical mixtures at $|t| \gg Gi$ and for distances $z \ll \xi_0 Gi^{-\nu}$. The crossover adsorption theory does not include the higher order corrections to $P(x)$ described by Eqs. (11)–(13). It is not yet understood how the higher order corrections to $P(x)$ compare with the mean field contributions in the differing reduced temperature and distance regimes.

III. EXPERIMENTAL METHODS

There are a number of experimental difficulties associated with neutron and x-ray experiments of strong critical adsorption that make these experiments somewhat difficult to implement. These difficulties could potentially explain some of the differences in the experimental results noted above and listed in Table I. Specifically, these difficulties include the following.

- (A) If one is studying the liquid-vapor surface of a critical liquid mixture, then, depending upon the cell design, the beam may have to pass through a macroscopic liquid meniscus at the entrance and exit windows of the sample cell because the incident beam is coming in at very small incident angles near grazing incidence. Differing groups have attempted to get around this meniscus problem in a number of different ways by (i) making the sample cell very long, which may create certain problems with regard to accurate temperature control, (ii) trying to account experimentally for this meniscus effect,³² or (iii) overfilling a sample cell such that the liquid-vapor surface sits above the sample cell lip.³⁴
- (B) If “strong” transverse thermal gradients are present (≥ 5 mK/cm), then convective flow within the liquid may perturb the adsorption profile at any surface.³⁷
- (C) Mechanical vibrations can perturb the reflected beam. Vibration problems are frequently minimized by making the bulk liquid sample very thin (<1 mm thick) so that longer wavelength capillary waves are damped out by the presence of the underlying solid cell wall.
- (D) Depending upon the scattering length density of the liquid mixture relative to the adjacent substrate (i.e., air or a solid), a large external critical angle may limit how close in temperature one can come to T_c .

For example, the critical wave vector is given by

$$Q_c = 4\sqrt{\pi\Delta\text{SLD}}, \quad (16)$$

where ΔSLD is equal to the difference in scattering length densities between the two adjacent bulk phases. Surface features of length scale ξ occur approximately at a wave vector

$$Q = \frac{2\pi}{\xi}. \quad (17)$$

Hence, for sufficiently large correlation lengths ξ (close to T_c), the critical adsorption features that one would like to study occur at very small Q . At the critical wave vector Q_c , the penetration depth (which determines the probe depth) is infinite. Thus very long range surface features are probed, but at extremely poor resolution in the vicinity of the critical edge. In order to investigate the scaling region close to T_c , one should therefore make Q_c very small. According to Eq. (16) small Q_c can be obtained by selecting similar scattering length densities for the substrate and liquid mixture where, in addition, one would also like good contrast between the adsorbed layer and the adjacent bulk phases. Figure 1 compares the relative benefits of small and large Q_c . Figure 1(a) shows neutron reflectivity data for a critical mixture of deuterated water plus 3-methylpyridine (W*P) against a crystalline

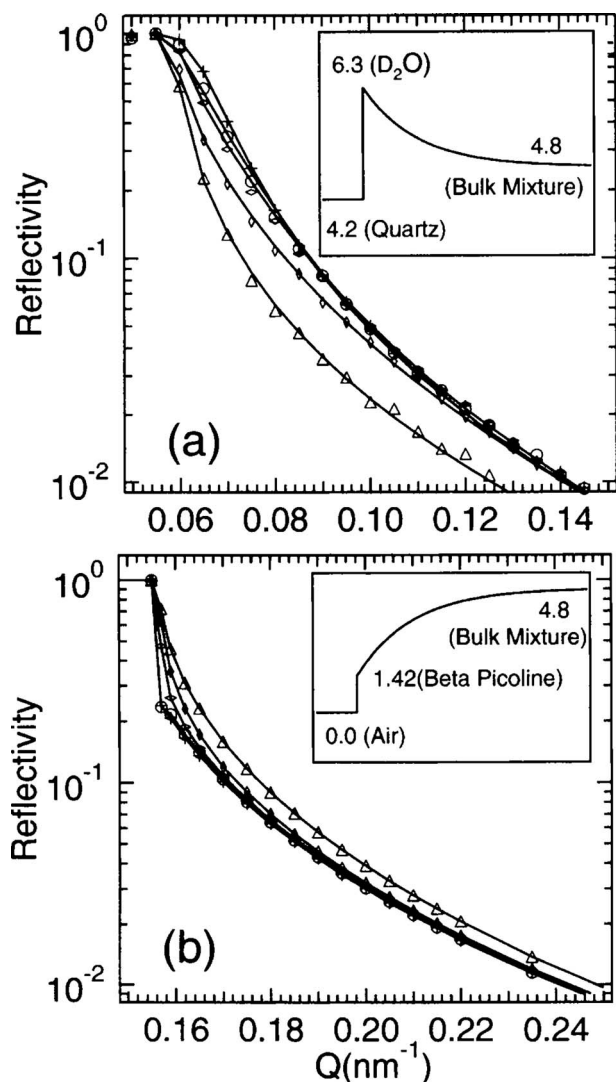


FIG. 1. Comparison between a critical mixture system with either a small or a large critical scattering vector, Q_c . (a) Experimental neutron data where Q_c is small for the critical mixture D_2O and 3-methylpyridine against a crystalline quartz substrate; D_2O adsorbs against the surface. The lines are fits to the data using the P1 model, as described in the text. (b) Computer calculations using the P1 model where Q_c is large for the same critical mixture against air. Here 3-methylpyridine adsorbs against the surface. For both (a) and (b), a schematic of the scattering length densities (in units of $10^{-4}/\text{nm}^2$) is shown in the insets. The differing neutron reflectivity curves possess temperature differences of $\Delta T = T_c - T = 0.08$ °C (crosses), 0.25 °C (circles), 0.5 °C (wide diamonds), 1.12 (tall diamonds), and 5.0 °C (triangles).

quartz substrate, which is studied later in this paper. This system possesses a small $Q_c \approx 0.06 \text{ nm}^{-1}$ because the scattering length densities of the two bulk phases are similar [Fig. 1(a), inset, and Table III]. The deuterated water, which adsorbs against the crystalline quartz substrate, provides good surface contrast relative to the two bulk phases. The solid

lines are fits to the experimental data using the P1 model, as will be described later. For this system one can readily distinguish all of the experimental reflectivity curves between $\Delta T = T_c - T = 0.08$ °C (crosses) and 5.0 °C (triangles). This behavior should be compared with a system possessing a large Q_c , obtained via computer calculations of the P1 model for the same critical mixture but now against air [Fig. 1(b)]. In this case, the 3-methylpyridine adsorbs at the surface because it possesses the lowest surface tension. $Q_c \approx 0.16 \text{ nm}^{-1}$ where there is a large drop in the reflectivity which is especially prominent for temperatures very close to T_c . The $\Delta T = 0.08$ °C (crosses) and 0.25 °C (circles) data are almost indistinguishable. Additionally, in a real neutron reflectometry experiment, because of the noise in the data and finite resolution in Q , it may be difficult in practice to distinguish between the 0.25 °C (circles) and 0.5 °C (wide diamonds) data. This behavior is reminiscent of an earlier x-ray reflectometry experiment,³⁴ completed by a couple of the current authors, from the liquid-air surface of the critical mixture tetrabromoethane+*n*-dodecane, where Q_c was large with a value of $\approx 0.28 \text{ nm}^{-1}$. In this experiment, it was found that the x-ray data for $\Delta T \lesssim 1$ °C could not be distinguished; hence, phenomena very close to T_c could not be studied.

The system W^*P against quartz, studied in this paper, has other advantages as well besides having a small Q_c . The neutrons are incident onto the surface through the small polished crystalline quartz substrate. Problems (A)–(C), mentioned above, are therefore eliminated. There is no liquid meniscus problem. The system is small; hence, it is easy to ensure that transverse thermal gradients are small. The solid substrate damps out any mechanical vibrations.

W^*P possesses a closed loop phase diagram with both an upper and a lower critical temperature. For convenience, we chose to work near the lower critical temperature ($T_c \approx 37$ °C) where the system was in the one (two) phase region for temperatures below (above) T_c . Deuterated water (isotropic purity of 99.96%, CAS [7789-20-0]) and 3-methylpyridine (99.5+ % pure, CAS [108-99-6]) were both obtained from Aldrich and used without any further purification. The critical mixture volume fraction of 69.1% deuterated water was determined using a standard volumetric procedure, where both phases have equal volumes in the two phase region for temperatures sufficiently close to the critical temperature T_c . In the present case, at 20 mK above T_c (in the two phase region), the volumes of the two phases were equal to within 2% which indicated a difference from the critical volume fraction of $\Delta\phi \leq 0.002$.

The sample cell consisted of a crystalline quartz substrate of width of 3.8, length of 8.3, and height of 1.3 cm and a stainless steel trough of depth of 3 mm. A Teflon encapsu-

TABLE III. Scattering length densities at 25 °C (from Ref. 40).

Substance	$10^4 \text{SLD} (\text{nm}^{-2})$	$10^7 (d\text{SLD}/dT) (\text{nm}^{-2} \text{K}^{-1})$
Crystalline quartz	4.18	
D_2O	6.37	-1.0
3-methylpyridine	1.43	-0.5
Critical mixture (at $\phi_{D_2O} = 0.691$)	4.84	

lated O-ring provided a seal between the quartz substrate and the trough. The measurable region of the interface was approximately $2 \times 5 \text{ cm}^2$. Two Teflon minivalves were used to access the cell. One valve was a fill port while the other valve enabled displaced air to exit the cell. The cell, substrate, and O-ring were separately sonicated in methanol, acetone, and ethanol, and then rinsed with distilled, de-ionized water. Both Teflon valves were similarly sonicated and purged thoroughly with distilled, de-ionized water. After 1 day in an oven at $110 \text{ }^\circ\text{C}$, the sample cell was assembled inside a laminar flow hood. The sample cell was filled at room temperature with the critical liquid mixture, leaving a bubble of $\sim 3 \text{ mm}$ diameter which subtended no more than 3% of the exposed substrate area. The cell was then elevated to a temperature of $35 \text{ }^\circ\text{C}$, which was $2 \text{ }^\circ\text{C}$ below the critical temperature. One valve was then opened to allow the cell pressure to come into equilibrium with the atmospheric pressure. The bubble was necessary to prevent a large buildup of pressure within the sample cell. In general the cell was tilted during measurements, thus removing the air bubble from the reflection region. The sample cell was contained in a temperature controlled environment similar to the one described in Ref. 38. The thermal stability was better than 2.0 mK/h , where thermal temperature gradients were less than 1 mK/cm . Three Yellow Springs Instrument 44034 thermistors were used, one for temperature control, and the other two, one at each end of the sample cell, for temperature and temperature gradient monitoring. The critical temperature was measured in the sample cell 3 days before the experiment and found to be $T_c = 37.055 \pm 0.01 \text{ }^\circ\text{C}$. The critical temperature was measured again 2 weeks after the experiment and had not drifted beyond the original range of uncertainty.

Beamline NG7 at the National Center for Neutron Research at the National Institute of Standards and Technology in Gaithersburg, MD was used to collect neutron reflectometry data at a neutron wavelength of $\lambda = 0.476 \text{ nm}$ for a wave vector step size of $0.005/\text{nm}$, which gave an uncertainty in the wave vector of $\Delta Q = \pm 0.0025/\text{nm}$. Measurements were taken at $\Delta T = T_c - T = 0.08, 0.25, 0.5, 1.12, 2.5, 5, 10, \text{ and } 20 \text{ }^\circ\text{C}$ below the critical temperature over a 4 day period. From these measurements the critical wave vector was found to be $Q_c = 0.059/\text{nm}$ for this crystalline quartz-critical mixture surface, which is in reasonable agreement with Eq. (16). The temperature range studied is much closer to T_c than was possible with any previous neutron or x-ray experiment, mainly because Q_c is so small. For each measurement the final set point temperature was approached from below. In each case, after giving the system 2 h or more to come into thermal equilibrium, two separate 1 h measurements were taken over the low part of the Q range. By comparing these measurements we could determine if the system had been given enough time to come into thermal equilibrium. Repeatability was tested by repeating our measurement at $\Delta T = 5 \text{ }^\circ\text{C}$, with an intervening measurement at $\Delta T = 2.5 \text{ }^\circ\text{C}$. Additionally, measurements taken on the last day of the experiment at $\Delta T = 10, 20, \text{ and } 0.5 \text{ }^\circ\text{C}$ were consistent with measurements taken during the first 2 days at $\Delta T = 5 \text{ and } 0.6 \text{ }^\circ\text{C}$. The first few reflectometry measurements were taken over a Q range of $0.04\text{--}0.61 \text{ nm}^{-1}$; however, background scattering

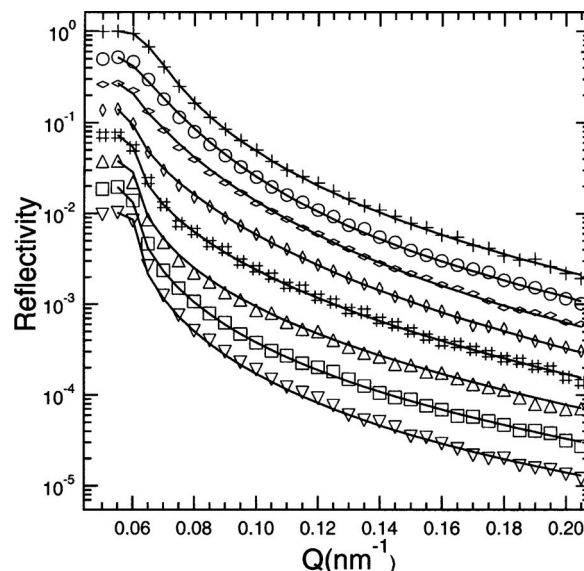


FIG. 2. Neutron reflectometry data taken at $\Delta T = 0.08$ (crosses), 0.25 (circles), 0.5 (wide diamonds), 1.12 (tall diamonds), 2.5 (number symbol), 5.0 (triangles), 10.0 (squares), and $20.0 \text{ }^\circ\text{C}$ (inverted triangles) for the critical mixture D_2O and 3-methylpyridine against a crystalline quartz substrate. The solid lines represent fits where the volume fraction of D_2O in the adsorbed surface layer is allowed to vary and the thickness of the adsorbed layer is fixed at $l_s = 0$ (see Table IV). The higher $\Delta T = 5.0, 10.0, \text{ and } 20.0 \text{ }^\circ\text{C}$ data can be equally well fitted for fixed $\phi_s = 0.896$ and variable l_s (Table IV) where no discernible difference in the fits can be observed (solid lines). For clarity each curve has been displaced vertically by a factor of 0.07 .

was found to dominate the data in the upper part of this range. Subsequent measurements were therefore restricted to a maximum Q of 0.25 nm^{-1} . The rms surface roughness of the crystalline quartz-air interface was measured in a separate experiment, using the same reflectometer, and found to have a value of $0.34 \pm 0.03 \text{ nm}$.

IV. ANALYSIS

The neutron reflectometry data R vs Q is shown in Fig. 2 at various temperatures. In this paper, the P1 model is compared with this neutron reflectometry data using the method suggested by Parratt.³⁹ For a given model, an effective refractive index profile $n(z)$ is approximated by a series of slabs of uniform refractive index. One then recursively solves Maxwell's equations for each interface, taking into account what happened at the previous interface. By this method one can approximate a profile and the resulting reflectivity curve, as precisely as one wishes. The refractive index for neutrons within a particular slab at depth z_i is given by

$$n(z_i) \approx 1 - \frac{\Omega \lambda^2}{2\pi} [\phi(z_i) \text{SLD}_{W^*} + (1 - \phi(z_i)) \text{SLD}_P], \quad (18)$$

where $\phi(z_i)$ is the local volume fraction of the adsorbed component (i.e., deuterated water), $\Omega = (V_{W^*} + V_P)/V_{W^*+P} \approx 1$ is the volume change on mixing, while SLD_{W^*} and SLD_P are the neutron scattering length densities of, respectively, deuterated water and 3-methylpyridine (Table III, Ref. 40). In this equation $\phi(z_i)$ is related to the surface scaling function $P_+(z_i)$ through Eqs. (1) and (2) with the function $P_+(z_i)$

TABLE IV. Fitting parameters.

ΔT (°C)	ϕ_s	l_s (nm)	$10^3 \Delta Q$ (nm ⁻¹)	χ^2	Ω
0.08	0.895	0.00	2.3±0.3	7.35	1
0.25	0.885	0.00	1.9±0.2	19.0	1
0.5	0.888	0.00	0.88±0.2	12.4	1
1.12	0.878	0.00	0.64±0.2	6.22	1
2.5	0.896	0.00	0.02	15.6	1
5	0.918	0.00 (fixed)	-0.04±0.2	20.8	1
10	0.939	0.00 (fixed)	0.34	8.85	1
20	0.998	0.00 (fixed)	0.48	24.6	1
5	0.896 (fixed)	0.482	-0.10±0.2	20.9	1
10	0.896 (fixed)	0.706	0.34	8.83	1
20	0.896 (fixed)	1.10	0.51	25.0	1
0.08	0.900	0	1.4	7.97	0.995

determined by the P1 model, namely, Eqs. (14) and (15) where the five parameters c_+ , c_{1+} , $P_{\infty+}$, P_{1+} , and x_0 are given in Table II. The system dependent parameters M_- and ξ_0 were determined by fitting the P1 model to ellipsometric data collected by Smith⁴¹ for this particular liquid mixture. The best fit values, $M_- = 0.7$ and $\xi_0 = 0.508$ nm, were in fair agreement with the values quoted in Ref. 41. In comparing the neutron reflectometry data with the P1 model, the only adjustable parameters occur in the vicinity of the surface at $z = 0$ where the P1 model must be joined in some manner onto the surface composition. Specifically, there were three adjustable parameters for each temperature, namely, the surface composition ϕ_s , the thickness of the surface layer l_s , and the extrapolation length z_e [Eq. (2)] which joins the P1 model smoothly onto the surface composition. One expects ϕ_s , l_s , and z_e to be similar for all temperatures. One also requires an additional adjustable parameter ΔQ , corresponding to a shift in Q , because in this experiment the critical wave vector Q_c is so small. We expect that ΔQ should be similar in magnitude to the instrumental resolution of ± 0.0025 nm⁻¹.

Following standard nonlinear least squares fitting procedures,⁴² the best fit to the experimental data is obtained by adjusting ϕ_s , l_s , z_e , and ΔQ for a minimum in χ^2 , where

$$\chi^2 = \sum_{j=1}^N \frac{[R_{P1}(Q_j) - R(Q_j)]^2}{\sigma_j^2}, \quad (19)$$

and $R_{P1}(Q_j)$ and $R(Q_j)$ are, respectively, the reflectivity for the P1 model and experimental neutron data at wave vector Q_j . In carrying out this fitting procedure one must take particular care in selecting the weight σ_j for each data point. If the standard weight $\sigma_j = \sqrt{R(Q_j)}$ is selected, then the high Q data points have insufficient impact on the overall fit, thus leading to an inaccurate picture of the profile. This difficulty arises because the reflectivity decreases by several orders of magnitude for increasing Q above Q_c . One must also be careful not to overweight the higher Q data points because then the fit becomes susceptible to the noise in the higher Q data. We examined a number of different measures for σ_j and found that

$$\sigma_j = R(Q_j) \sqrt{1 - \log_{10}(R(Q_j))} \quad (20)$$

gave results that were consistent over the entire Q range. The first term, in Eq. (20) [$R(Q_j)$], compensates for the differing orders of magnitude in the reflectivity between low and high Q data, while the second term decreases the weighting for the noisier higher Q data.

We modeled our system with an intermediate layer of thickness l_s and constant composition ϕ_s (the surface layer referred to above) between our quartz substrate and the P1 decay model of Carpenter *et al.* The inclusion of the intermediate layer was inspired from the results in Ref. 34. The extrapolation length z_e , which is generally chosen such that $\phi(z=0) = 1$, was instead chosen such that the P1 decay profile would begin with a composition of ϕ_s . In our initial fits l_s was allowed to vary from 0 (i.e., no intermediate film) to 2 nm. The best fits for $\Delta T = 0.08, 0.25, 0.5, 1.12,$ and 2.5 °C, consistent with the idea that l_s and ϕ_s should be independent of temperature, were obtained with a surface thickness $l_s = 0$ nm for the adsorbed film and a surface volume fraction $\phi_s \equiv \phi_{D_2O}(z=0)$ between 0.878 and 0.896. These fits indicate that no intermediate film is necessary and the P1 model alone suffices to describe the behavior within 2.5 °C of the critical temperature. The best fit to the 5 °C data also had an intermediate layer thickness of 0 nm, but in this case $\phi_s = 0.918$, outside the range for fits at temperatures nearer to T_c . This trend of increasing ϕ_s continues at 10 and 20 °C. In all cases where the intermediate layer is of zero thickness, the layer serves only to control the initial value of ϕ in the P1 decay profile. These results are tabulated in Table IV and fits are displayed in Fig. 2 (solid line). The higher $\Delta T \geq 5$ °C data can also be equally well fitted with an alternative model where ϕ_s is held constant at 0.896 and l_s is varied. This alternative model possesses a similar χ^2 and cannot visually be distinguished from the previous $l_s = 0$ model with variable ϕ_s (Fig. 2). Undoubtedly, the $\Delta T \geq 5$ °C experimental data could be equally well fitted by some combination of these two models. This break down of the model of Carpenter *et al.* further from T_c is perhaps not surprising as, in this region, a crossover to the mean field behavior is expected.³⁶ However, it should be noted that this break down of the model of

Carpenter *et al.*, exhibited by the neutron measurements far from T_c , does not negate the ellipsometric results of Carpenter *et al.*⁴ which were primarily sensitive to surface structural variations within 1 °C of T_c .

Within 2.5 °C of T_c the model of Carpenter *et al.* with no intermediate layer ($l_s=0$) and $\phi_s=0.887\pm 0.009$ provides a good description of the experimental data. A surprising result of this analysis is that $\phi_s \neq 1$, which would seem to indicate weak adsorption, although fits to the weak critical adsorption scaling equations in Ref. 7 provided unsatisfactory results. The likely physical reason for this partial surface saturation, with $\phi_{D_2O}(z=0) \approx 0.887$, is the competing hydrogen bonding with the surface between deuterated water and 3-methylpyridine [3-CH₃(C₅H₄N)]. This model of Carpenter *et al.* close to T_c provides a good but not perfect description of the experimental data as the results in Table IV exhibit a small systematic trend in the wave vector shift ΔQ as one approaches T_c . This trend is *small* and falls within the wave vector uncertainty of $\pm 0.0025/\text{nm}$. The small critical wave vector $Q_c=0.059/\text{nm}$, for our system, undoubtedly makes this small ΔQ shift visible. There are a number of potential causes for this small systematic trend in ΔQ .

- (i) Our sample cell and temperature controlled environment are made of a number of disparate materials, including aluminum, stainless steel, crystalline quartz, a Teflon encapsulated O-ring, and nylon capped set screws each with their own differing thermal expansion coefficients. A rotation of 0.006° would suffice to account for the apparent range in ΔQ . We cannot rule out this possibility.
- (ii) In the above neutron analysis as well as the ellipsometric analysis of Carpenter *et al.*,¹ it was assumed that the volume change on mixing $\Omega=(V_{W^*}+V_P)/V_{W^*+P}=1$. This is a reasonable approximation to within 1% or 2%;⁴³ however, a $\Omega \neq 1$ could potentially explain the small ΔQ trend exhibited in Table IV for $\Delta T \leq 2.5$ °C. Kayser⁴³ found that $\Omega = 0.983 \pm 0.036(-t)^\beta$ in the two phase region of the critical binary liquid mixture nitromethane+carbon disulfide. As far as we are aware, the temperature behavior of Ω in the one phase region has not been studied. A small deviation of Ω from 1.00 significantly influences the value of ΔQ . For example, we have examined the influence of $\Omega=0.995$ in Table IV for $\Delta T=0.08$ °C. This small deviation of Ω from 1.00 significantly alters the value of ΔQ while only marginally changing the value of ϕ_s . Hence, the ΔQ trend for the model of Carpenter *et al.* (with $l_s=0$) at $\Delta T \leq 2.5$ °C could be due to this little understood parameter Ω .

In this experiment Q_c is small. One therefore needs to carefully consider the instrumental resolution and how this might influence the results. Q depends upon both λ and the incident angle θ . The beam is not perfectly monochromatic. Additionally, the finite size of the beam, sample, and detector assure that there will be a range of θ values within the beam. Thus, for a given data point, one is measuring R over a range of values $Q \pm \Delta Q/2$. Resolution depends on the ratios $\Delta\lambda/\lambda$

and $\Delta\theta/\theta$. For the NG7 reflectometer $\Delta\lambda/\lambda=0.025$. For the geometry of our system we calculate that $\Delta\theta/\theta=0.025$. Simulations demonstrated that even doubling the calculated value of $\Delta\theta/\theta$ had a negligible influence on the results. The relatively small size of our sample has assisted us in this regard.

V. SUMMARY

In this paper, we have found good agreement between critical adsorption results for a neutron reflectometry experiment on the critical mixture deuterated water plus 3-methylpyridine against a crystalline quartz substrate within 2.5 °C of T_c and the analysis of Carpenter *et al.*⁴ on ellipsometric data taken on similar systems. This agreement differs from much of the previous neutron and x-ray literature on strong critical adsorption at the surfaces of critical binary mixtures, as summarized in Table I, where in many cases there is disagreement between the various x-ray, neutron, and ellipsometry experiments as well as theory. One unexpected result, which has arisen from this work, is that the surface composition ϕ_s of the preferentially adsorbed component (in this case deuterated water) is not completely saturated, as is normally assumed for strong critical adsorption. More specifically we have found that the surface volume fraction of deuterated water is $\phi_s \approx 0.89$ for this particular system. We attribute this partial saturation to competing hydrogen bonding for the crystalline quartz surface between deuterated water and 3-methylpyridine.

A novelty introduced in this work, which enabled us to get much closer to the critical temperature T_c than previous x-ray or neutron studies, was the use of a crystalline quartz substrate which was closely matched to the scattering length density of the critical liquid mixture. This choice gave rise to a very small critical wave vector $Q_c \sim 0.06 \text{ nm}^{-1}$ which enabled us to probe very large length scales (corresponding to small reduced temperatures t) in a region where scaling is expected to hold. A limitation of the current work is that reflectivity data could only be collected out to a maximum Q of $\sim 0.25 \text{ nm}^{-1}$. Reflectivity data collected from our system at higher Q were dominated by bulk liquid background scattering. There is still room for improvement in our experimental design. A very thin liquid sample would allow us to collect reflectivity data at very large Q because such a cell would minimize the background scattering.⁴⁴ Such an improvement would provide superior resolution of the small length scale interfacial features.

ACKNOWLEDGMENTS

One of the authors (B.M.L.) acknowledges support for this work from the U.S. Department of Energy through Grant No. DE-FG02-02ER46020 and partial support through the U.S. National Science Foundation through Grant No. DMR-0603144. Oak Ridge National Laboratory is managed for the U.S. Department of Energy under Contract No. DE-AC05-00OR22725 by UT-Battelle LLC. The authors acknowledge valuable discussions with Greg Smith on various neutron reflectometry related issues.

- ¹A. W. Adamson, *Physical Chemistry of Surfaces* (Wiley, New York, 1982).
- ²M. E. Fisher and P.-G. de Gennes, C. R. Seances Acad. Sci., Ser. B **287**, 207 (1978).
- ³M. E. Fisher and J.-H. Chen, J. Phys. (Paris) **46**, 1645 (1985).
- ⁴J. H. Carpenter, B. M. Law, and D. S. P. Smith, Phys. Rev. E **59**, 5655 (1999); J. H. Carpenter, J.-H. J. Cho, and B. M. Law, *ibid.* **61**, 532 (2000).
- ⁵M. E. Fisher and H. Au-Yang, Physica A **101**, 255 (1980); H. Au-Yang and M. E. Fisher, Phys. Rev. B **21**, 3956 (1980).
- ⁶U. Ritschel and P. Czerner, Phys. Rev. Lett. **77**, 3645 (1996).
- ⁷J.-H. J. Cho and B. M. Law, Phys. Rev. Lett. **86**, 2070 (2001); Phys. Rev. E **65**, 011601 (2001).
- ⁸P. Frodl and S. Dietrich, Phys. Rev. E **48**, 3741 (1993).
- ⁹J.-H. J. Cho and B. M. Law, Phys. Rev. Lett. **89**, 146101 (2002); **67**, 031605 (2003).
- ¹⁰A. I. Rusanov, Prog. Surf. Membr. Sci. **4**, 57 (1971).
- ¹¹D. Beaglehole, in *Fluid Interfacial Phenomena*, edited by C. A. Croxton (Wiley, New York, 1986).
- ¹²D. Beaglehole, J. Chem. Phys. **73**, 3366 (1980); **75**, 1544 (1981).
- ¹³B. Heidel and G. H. Findenegg, J. Phys. Chem. **88**, 6575 (1984); J. Chem. Phys. **87**, 706 (1987); R. Süßmann and G. H. Findenegg, Physica A **156**, 114 (1989).
- ¹⁴J. W. Schmidt and M. R. Moldover, J. Chem. Phys. **83**, 1829 (1985).
- ¹⁵J. W. Schmidt, Phys. Rev. A **41**, 885 (1990).
- ¹⁶C. Franck and S. E. Schnatterly, Phys. Rev. Lett. **48**, 763 (1982); C. Franck, J. Chem. Phys. **82**, 5633 (1985); J. A. Dixon, M. Schlossman, X.-L. Wu, and C. Franck, Phys. Rev. B **31**, 1509 (1985).
- ¹⁷M. Schlossman, X.-L. Wu, and C. Franck, Phys. Rev. B **31**, 1478 (1985).
- ¹⁸D. Beysens and S. Leibler, J. Phys. (Paris), Lett. **43**, L133 (1982).
- ¹⁹S. Blümel and G. H. Findenegg, Phys. Rev. Lett. **54**, 447 (1985).
- ²⁰D. S. P. Smith and B. M. Law, Phys. Rev. E **52**, 580 (1995); **54**, 2727 (1996).
- ²¹A. J. Liu and M. E. Fisher, Phys. Rev. A **40**, 7202 (1989).
- ²²H. W. Diehl and M. Smock, Phys. Rev. B **47**, 5841 (1993); **48**, 6470(E) (1993).
- ²³M. Smock, H. W. Diehl, and D. P. Landau, Ber. Bunsenges. Phys. Chem. **98**, 486 (1994).
- ²⁴Z. Borjan and P. J. Upton, Phys. Rev. E **63**, 065102(R) (2001).
- ²⁵G. Flöter and S. Dietrich, Z. Phys. B: Condens. Matter **97**, 213 (1995).
- ²⁶D. S. P. Smith and B. M. Law, Phys. Rev. E **55**, 620 (1997).
- ²⁷J.-H. J. Cho, B. M. Law, and K. Gray, J. Chem. Phys. **116**, 3058 (2002).
- ²⁸J.-H. J. Cho and B. M. Law, Phys. Rev. E **72**, 041601 (2005).
- ²⁹S. Dietrich and R. Schack, Phys. Rev. Lett. **58**, 140 (1987).
- ³⁰H. Zhao, A. Penninckx-Sans, L.-T. Lee, D. Beysens, and G. Jannink, Phys. Rev. Lett. **75**, 1977 (1995).
- ³¹J. R. Howse, J. Bowers, E. Manzanares-Papayanopoulos, I. A. McLure, and R. Steitz, Phys. Rev. E **59**, 5577 (1999).
- ³²J. Jestin, L.-T. Lee, M. Privat, and G. Zalczler, Eur. Phys. J. B **24**, 541 (2001).
- ³³J. Bowers, A. Zorbakhsh, H. K. Christenson, I. A. McLure, J. R. P. Webster, and R. Steitz, Phys. Rev. E **72**, 041606 (2005).
- ³⁴L. W. Marschand, M. Brown, L. B. Lurio, B. M. Law, S. Uran, I. Kuzmenko, and T. Gog, Phys. Rev. E **72**, 011509 (2005).
- ³⁵S. B. Kiselev, L. Lue, and M. Yu. Belyakov, Phys. Lett. A **251**, 212 (1999); **260**, 168 (1999); S. B. Kiselev, J. F. Ely, and M. Yu. Belyakov, J. Chem. Phys. **112**, 3370 (2000).
- ³⁶J. K. Whitmer, S. B. Kiselev, and B. M. Law, J. Chem. Phys. **123**, 204720 (2005).
- ³⁷D. S. P. Smith (unpublished).
- ³⁸M. Brown, S. Uran, B. Law, L. Marschand, L. Lurio, I. Kuzmenko, and T. Gog, Rev. Sci. Instrum. **75**, 2536 (2005).
- ³⁹L. G. Parratt, Phys. Rev. **95**, 359 (1954).
- ⁴⁰A. Munter, scattering length density calculator (<http://www.ncnr.nist.gov/resources/sldcalc.html>).
- ⁴¹D. S. P. Smith and B. M. Law, J. Chem. Phys. **99**, 9836 (1993).
- ⁴²R. P. Bevington and D. K. Robinson, *Data Reduction and Error Analysis for the Physical Sciences*, 2nd ed (McGraw-Hill, New York, 1992).
- ⁴³R. F. Kayser, Phys. Rev. B **34**, 3254 (1986).
- ⁴⁴J. Majewski (private communication).